Available online at www.sciencedirect.com
SCIENCE DIRECT
Journal of Molecular Catalysis A: Chemical 252 (2006) 40–48
JOURNAL OF MOLECULAR CATALYSIS A: CHEMICAL
www.elsevier.com/locate/molcata

The effect of iron oxides and oxalate on the photodegradation of 2-mercaptobenzothiazole

Chengshuai Liu [a,b,c], Fangbai Li [b,*], Xiaomin Li [a,b,c], Gan Zhang [a], Yaoqiu Kuang [a]

[a] *Guangzhou Institute of Geochemistry, Chinese Academy of Sciences, Guangzhou 510640, PR China*
[b] *Guangdong Key Laboratory of Agricultural Environment Pollution Integrated Control, Guangdong Institute of Eco-Environment and Soil Science, Guangzhou 510650, PR China*
[c] *Graduate School of the Chinese Academy of Sciences, Beijing 100039, PR China*

Received 25 October 2005; received in revised form 11 January 2006; accepted 6 February 2006
Available online 15 March 2006

Abstract

γ-FeOOH was prepared by hydrothermal process and went through the phase transformation from lepidocrocite to maghemite firstly and then to hematite with the increase of sintering temperature. The iron oxides sintered at 250, 320, 420 and 520 °C for 2 h were named as IO-250, IO-320, IO-420 and IO-520, respectively, and characterized by X-ray diffractograms (XRD) and Brunauer–Emmett–Teller (BET) methods. XRD results showed that IO-250 and IO-320 had a mixed crystal structure of maghemite and hematite while IO-420 and IO-520 were pure hematite. BET results showed that the specific surface area decreased significantly with the increase of sintering temperature. The effect of iron oxides and oxalate on the photodegradation of 2-mercaptobenzothiazole (MBT) was investigated. The degradation of MBT depended strongly on the dosage of iron oxides and the initial concentration of oxalic acid (C^0_{ox}). The optimal dosages of iron oxides were 0.40, 0.35, 0.30, 0.25 and 0.25 g/L for γ-FeOOH, IO-250, IO-320, IO-420 and IO-520, respectively, and the optimal C^0_{ox} was 1.0 mM for all the five iron oxides. The results showed that MBT photodegradation could be enhanced greatly in the presence of oxalic acid. The first-order kinetic constants k for MBT degradation was ranked the order as IO-320 > IO-250 > IO-420 > IO-520 > γ-FeOOH in the presence of oxalate with the optimal C^0_{ox} of 1.0 mM. The oxalate photodegradation, the pH value in the solution and the concentration of Fe^{2+} and Fe^{3+} along with the reaction time were also investigated. The results showed that they also depended on iron oxides and C^0_{ox}. IO-420 and IO-520 with hematite structure and higher stability had a lower activity for oxalate adsorption and photodegradation, and then less formation of Fe^{3+} and Fe^{2+}, while γ-FeOOH and IO-250 with a lower stability had much higher activity for oxalate adsorption and photodegradation, and then much more Fe^{3+} and Fe^{2+} formed in the solution. The excessive Fe^{3+} inhibited the formation of H_2O_2 while the much less $Fe^{2+/3+}$ led to a much less $Fe^{2+/3+}$-oxalate complex on the surface of iron oxides or in the solution. Therefore, IO-320 had the most photoactivity among them because of the mixed crystal structure and the suitable concentration of Fe^{3+} and Fe^{2+}.

Keywords: Photodegradation; Iron oxide; Oxalic acid; 2-Mercaptobenzothiazole; UVA light

1. Introduction

Fenton system has been paid for much attention over the past several decades [1–5] because of its powerful ability of degradation of organic pollutants (abbreviated as OPs). In Fenton system, the generation of hydroxyl radical (•OH) is the key step because hydroxyl radical can oxidize almost all organic matters and mineralize them to carbon dioxide and water owing to its high oxidation potential ($E^0 = +2.80$ V) [6,7]. In the last decade years, ozone [8,9], electricity [10–12] and light [7,13,14] were introduced into Fenton system to form a so-called Fenton-like system and to increase the efficiency of generation of •OH. In Fenton and Fenton-like systems, hydrogen peroxide (H_2O_2) is the most important factor because it is the direct source of •OH [15]. Sufficient hydrogen peroxide has to be added so as to make the system be efficient [3,16]. However, H_2O_2 is an acute reactive reagent and cannot stand in nature for a long time. This factor limits the application of Fenton and Fenton-like system in the remediation of OPs in nature.

In fact, iron oxides and oxalic acid, which coexisted in natural environments, can set up a Fenton-like system without additional H_2O_2 [17–19]. Iron is the fourth most abundant

* Corresponding author. Tel.: +86 20 87024721; fax: +86 20 87024123.
E-mail address: cefbli@soil.gd.cn (F. Li).

1381-1169/$ – see front matter © 2006 Elsevier B.V. All rights reserved.
doi:10.1016/j.molcata.2006.02.036

element of the earth's crust (5.1 mass%). Iron oxides (including oxyhydroxides) should be a kind of natural minerals and geocatalysts. The iron oxides are found in soils and rocks, lakes and rivers, on the seafloor, in air and organism [20]. Major iron oxides include goethite (α-FeOOH), hematite (α-Fe_2O_3), maghemite (γ-Fe_2O_3), lepidocrocite (γ-FeOOH) and magnetite (Fe_3O_4). In natural conditions, hematite usually exists together with maghemite. On the other hand, oxalic acid has strong chelating ability with multivalent cations and is mainly exuded by plants in natural environment [21]. Oxalic acid is also an intermediate in the catalytic oxidation of phenol [22–25], and coumaric acid as a by-product of oil manufacturing [26]. In a word, this Fenton-like oxidation process can utilize natural mater (iron oxides and oxalic acid) without additional H_2O_2 and artificial injection of iron and should be a very important way of OPs decontamination in natural environment. It is meaningful to investigate the photochemical reaction in the iron oxide–oxalate complex system for understanding the natural transformation of organic pollutants. In fact, the photochemistry of Fe(III)-oxalate complexes in natural aquatic environment, fog, precipitation, tropospheric aerosols and soil solution has received considerable attention over the past three decades [27–32] because iron oxide–oxalate exhibit strong ligand-to-metal charge absorption bands in the UVA region. But, to our best knowledge, there is little report on the photodegradation of OPs in the system consisting of iron oxide minerals and oxalic acid.

In this study, 2-mercaptobenzothiazole (MBT) was selected as the model pollutant because it is the most important member of the benzothiazole group of heterocyclic aromatic compounds. This xenobiotic compound is used mainly in the manufacture of rubber as additive chemicals [33] but also has other uses, notably as a corrosion inhibitor [34]. MBT enters the environment from factories producing and using it and from products containing it [35]. MBT has been shown to induce tumors, to be allergenic, to be toxic to aquatic organisms, to hamper wastewater treatment, and also to inhibit degradation of easily degradable OPs [36]. So, its removal from environment has caused for much concern [37–40]. But little attention has been devoted to the research of the photocatalytic degradation of MBT in the iron oxide–oxalate complex system. The objective of this study is to investigate the effect of iron oxides and oxalic acid on MBT photodegradation; and the effect of the variation of the pH value and the formation of Fe^{2+} and Fe^{3+} on MBT photodegradation during the photochemical process.

2. Experimental

2.1. Preparation of iron oxides

γ-FeOOH was prepared by hydrothermal method described previously [41]. First, 16 g of $FeCl_2{\cdot}4H_2O$, 22.4 g of $(CH_2)_6N_4$ and 5.6 g of $NaNO_2$ were dissolved in 400, 80 and 80 mL of double-distilled water, respectively. Then the three solutions were mixed to obtain a bluish green precipitate. The precipitate was aged in the mixture at 60 °C for 3 h before it was centrifuged. The precipitate was washed three times with alcohol and distilled water to remove anions and organic impurities and then dried at 65 °C for 48 h. The dried gel was ground and an orange-colored γ-FeOOH was obtained. Then, γ-FeOOH powder was sintered at 250, 320, 420 and 520 °C for 2 h, respectively, at 2 °C/min temperature increase rate and the products were named as IO-250, IO-320, IO-420 and IO-520 accordingly.

2.2. Characterization of iron oxides

The X-ray powder diffraction patterns of the five iron oxides were recorded on a Rigaku D/Max-III A diffract meter at room temperature, operating at 30 kV and 30 mA, using a Cu Kα radiation (λ = 0.15418 nm). The phases were identified by comparing diffraction patterns with those on the standard powder XRD cards compiled by the Joint Committee on Powder Diffraction Standards (JCPDS) [42]. The total surface area and total pore volume of five samples were measured by the Brunauer–Emmett–Teller (BET) method in which the N_2 adsorption at 77 K was applied and Carlo Erba Sorptometer was used [43].

2.3. Experiment of MBT photodegradation

The photodegradation of MBT was carried out using a Pyrex cylindrical photoreactor, of which an 8 W black light lamp (Luzchem Research Inc.) with the main emission at 365 nm was positioned at the centre. The photoreactor was surrounded by a Pyrex circulation water jacket to control the temperature during reaction and was covered by aluminum foil to avoid indoor light irradiation. The reaction suspension was formed by adding given dosage of iron oxide powder into 250 mL of aqueous MBT solution. In all experiments here the initial concentration of MBT was 10 mg/L. Prior to the photoreaction, the suspension was magnetically stirred in the dark for 30 min to establish adsorption/desorption equilibrium. During the photoreaction process, the aqueous suspension was irradiated by the UVA light with constant aeration and magnetically stirring. And at the given time intervals, the analytical samples were withdrawn from the suspension and immediately centrifuged for 20 min at 4800 rpm and then stored in the dark for needed analysis.

2.4. Analytical method

The remaining MBT during the photodegradation was determined by liquid chromatography (LC). A mobile phase consisting of 70% methanol (HPLC grade) and 30% water (HPLC grade) acidified by adding 1% (v/v) acetic acid was operated at a flow rate of 0.5 mL/min, and a wavelength of 323 nm was used to detect MBT. The concentration of oxalic acid during photoreaction was determined by ion chromatography (Dionex DX-120). An IONPAC ASII-AC and AGII-HC (4 nm) were used for analysis, in which mobile phase consisting of 15 mmol/L KOH solution was operated at a flow rate of 1.0 mL/min with the retention time of 7.08 min for oxalic acid. The concentration of Fe^{3+} and Fe^{2+} ions were tested by the 1, 10-phenanthroline method [44].

3. Results and discussion

3.1. Properties of iron oxides

Fig. 1 showed the X-ray diffractograms (XRD) of iron oxides. Pure γ-FeOOH powder was obtained firstly because all eight peaks of (0 2 0), (1 2 0), (0 3 1), (1 1 1), (2 0 0), (2 2 0), (1 5 1) and (2 3 1) determined by XRD were attributable to γ-FeOOH. IO-420 and IO-520 were pure hematite because nine peaks of (0 1 2), (1 0 4), (1 1 0), (1 1 3), (0 2 4), (1 1 6), (0 1 8), (2 1 4) and (3 0 0) were attributable to hematite [45]. At meantime, IO-250 and IO-320 should consist of the mixture of maghemite and hematite. The strongest XRD peak of hematite is the (1 0 4) peak with the d_{hkl}-values of 2.69 while that of maghemite is the (3 1 1) peak with the d_{hkl}-values of 2.518. However, the peak (1 1 0) with the d_{hkl}-values of 2.51 for hematite and the peak (3 1 1) for maghemite present at the same position of Bragg angles. For IO-250 and IO-320, the strongest peak at $2\theta = 35.7^\circ$ should contain two peaks (1 1 0) and (3 1 1), and the second strongest peak at $2\theta = 33.2^\circ$ should be attributable to hematite (1 0 4) peak because (1 1 0) peak is the second strongest peak, not the first strongest peak for hematite standard graph, as showed in Fig. 1. Furthermore, for IO-250 and IO-320, the peaks (4 2 2) and (4 4 0) of maghemite at $2\theta = 52.2$ and 62.8°, respectively, were also almost at the same position of peaks (1 1 6) and (2 1 4) of hematite, respectively. IO-250 and IO-320 also had two small (4 2 2) and (4 4 0) peaks at $2\theta = 52.2$ and 62.8°, respectively, which attributed to maghemite, but hematite. It is difficult to determine the relative ratio of (1 1 0) peak for hematite and (3 1 1) peak for maghemite. Obviously, the content of hematite increased with the increase of sintering temperature because the relative intensity of (1 0 4) peak for hematite increased with the increase of sintering temperature. It could be concluded that the phase transformation from lepidocrocite to maghemite and then to hematite occurred gradually with the increase of sintering temperature. The crystal size of γ-FeOOH, IO-250, IO-320, IO-420 and IO-520 were 13.7, 19.2, 35.7, 54.7 and 73.9 nm deduced from Sherrer's formula with their strongest peaks of XRD based on Fig. 1. Obviously, the crystal size increased with increasing the sintering temperature.

The specific surface area and total pore volume of iron oxides samples were measured by BET method. The specific surface area of γ-FeOOH, IO-250, IO-320, IO-420 and IO-520 was 115.44, 75.91, 60.48, 29.40 and 22.11 m^2/g, respectively; while the total pore volume was 0.2977, 0.3485, 0.3762, 0.2747 and 0.1650 m^3/g, respectively. The results showed that the specific surface area decreased with increasing the sintering temperature. γ-FeOOH had the largest specific surface area while IO-320 had the largest total pore volume.

3.2. Photodegradation of MBT on different conditions

Fig. 2 showed the MBT degradation on the different conditions. Without UV light (dark) and only with 1.0 mM oxalic acid and 0.4 g/L IO-420 in the 250 mL suspension, the concentration of MBT decreased slightly at 1.9% because of adsorption on the surface of iron oxide (curve a). The removal percentage of MBT was at 7.8% level under UV light irradiation without iron oxide and oxalic acid (curve b), and at 12% level at 90 min under UV light with 0.4 g/L IO-420 and without oxalic acid (curve c). When both 1.0 mM oxalic acid and iron oxide with 0.4 g/L dosage were added into the reaction suspension to form the photo-Fenton-like system under UV irradiation (curves d–h), the removal percentage of MBT was significantly increased, and was up to 41.0, 78.9, 89.5, 76.3 and 67.5%. The degradation of MBT in iron oxide–oxalate systems can be described by first-order kinetic well and the first-order kinetic constants k were 0.75×10^{-2} ($R = 0.9571$), 2.01×10^{-2} ($R = 0.9846$), 2.74×10^{-2} ($R = 0.9934$), 1.84×10^{-2} ($R = 0.9886$) and 1.5×10^{-2} ($R = 0.9868$) min^{-1} for γ-FeOOH, IO-250, IO-

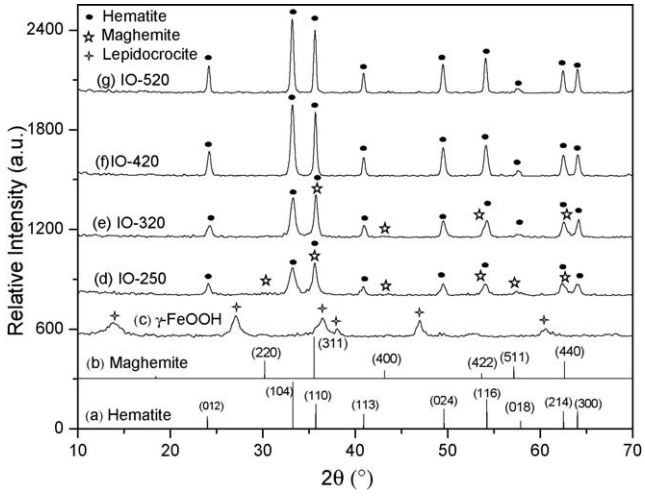

Fig. 1. The XRD graph of iron oxides powders (curves a and b were the standard XRD graphs of hematite and maghemite, respectively).

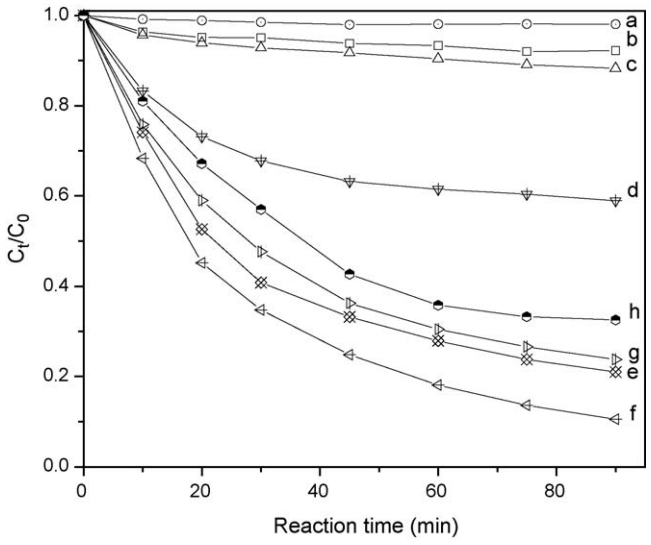

Fig. 2. Photodegradation of 10 mg/L MBT under different conditions: (a) 1.0 mM oxalic acid + 0.4 g/L IO-420, (b) UV, (c) UV + 0.4 g/L IO-420, (d) 0.4 g/L γ-FeOOH + UV + 1.0 mM oxalic acid, (e) 0.4 g/L IO-250 + 1.0 mM oxalic acid + UV, (f) 0.4 g/L IO-320 + 1.0 mM oxalic acid + UV, (g) 0.4 g/L IO-420 + 1.0 mM oxalic acid + UV and (h) 0.4 g/L IO-520 + 1.0 mM oxalic acid + UV.

320, IO-420 and IO-520, respectively, after 90 min reaction. Obviously, the k value was ranked as the order of IO-320 > IO-250 > IO-420 > IO-520 > γ-FeOOH. The results showed that iron oxides, oxalate and UV light all should play important roles in MBT degradation, and MBT photodegradation should be greatly enhanced in the cooperation of iron oxide and oxalate. At the meantime, MBT photodegradation also strongly depended on the properties of iron oxides. Among of iron oxides, IO-320 had the most photochemical activity. Because IO-320 had a mixed crystal structure of maghemite and hematite and the largest total pore volume. Actually the band gaps of maghemite (2.03 eV) and hematite (2.02 eV) are very close, but they have different positions. Hematite has a conduction band level at −0.62 V and a valence band level at +1.40 V, while maghemite has a conduction band level at −0.08 V and a valence band level at +1.94 V [46]. The mixed crystal structure should result in an effective electron separation and transformation within the iron oxides. On the other hand, the conditions such as pH value and the concentration of Fe^{2+} and Fe^{3+} in the IO-320-oxalate system may favor the degradation of MBT in the system, as discussed behind.

3.3. The dependence of MBT photodegradation on the dosage of iron oxides

Fig. 3 showed the dependence of MBT degradation on the dosage of IO-420 in the presence of oxalic acid with an initial concentration of 1.0 mM. The first-order kinetic constants k was 1.65×10^{-2} ($R = 0.9922$), 1.97×10^{-2} ($R = 0.9858$), 2.06×10^{-2} ($R = 0.9854$), 1.85×10^{-2} ($R = 0.9908$), 1.84×10^{-2} ($R = 0.9886$), 1.09×10^{-2} ($R = 0.9830$) and 0.91×10^{-2} ($R = 0.9867$) min^{-1} with the dosage of 0.10, 0.20, 0.25, 0.30, 0.40, 1.00 and 1.50 g/L, respectively. Obviously, there should be an optimal dosage of 0.25 g/L for IO-420. In fact, excessive dosage of iron oxide will limit the penetration of UV light in the solution and lead to the quick decay of UV light intensity. The similar results could be obtained by using other iron oxides.

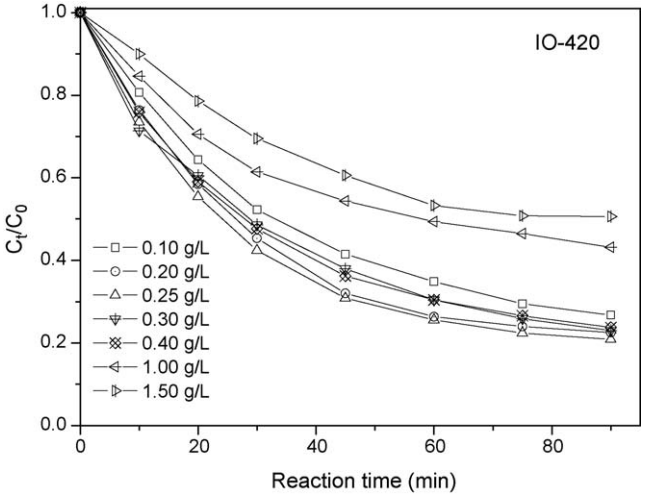

Fig. 3. The effect of IO-420 dosage on the photodegradation of 10 mg/L MBT under UV irradiation in the presence of 1.0 mM oxalic acid.

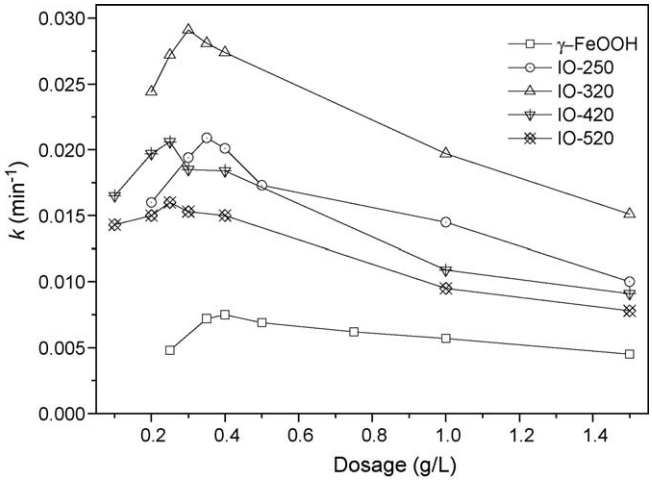

Fig. 4. The first-order reaction kinetic constants (k) vs. the dosage of different iron oxides in the presence of 1.0 mM oxalic acid under UV irradiation.

Fig. 4 showed that the dependence of the first-order kinetic constants (k) on the dosage of the five kinds of iron oxides in the presence of oxalic acid with an initial concentration of 1.0 mM. The k values of MBT degradation were up to 0.75×10^{-2}, 2.09×10^{-2}, 2.91×10^{-2}, 2.06×10^{-2} and 1.6×10^{-2} min^{-1} when the optimal dosage were 0.40, 0.35, 0.30, 0.25 and 0.25 g/L by using γ-FeOOH, IO-250, IO-320, IO-420 and IO-520, respectively.

3.4. The dependence of MBT photodegradation on the initial concentration of oxalate

Fig. 5 showed the dependence of MBT photodegradation on the initial concentration of oxalic acid (C_{ox}^0) with the dosage of 0.4 g/L IO-420 under UV light irradiation. The k values of MBT degradation were 0.11×10^{-2} ($R = 0.9609$), 0.82×10^{-2} ($R = 0.9767$), 1.11×10^{-2} ($R = 0.9747$), 1.37×10^{-2} ($R = 0.9834$), 1.84×10^{-2} ($R = 0.9886$), 1.56×10^{-2} ($R = 0.9864$), 1.06×10^{-2} ($R = 0.9736$), 0.88×10^{-2} ($R = 0.9691$) and 0.76×10^{-2}

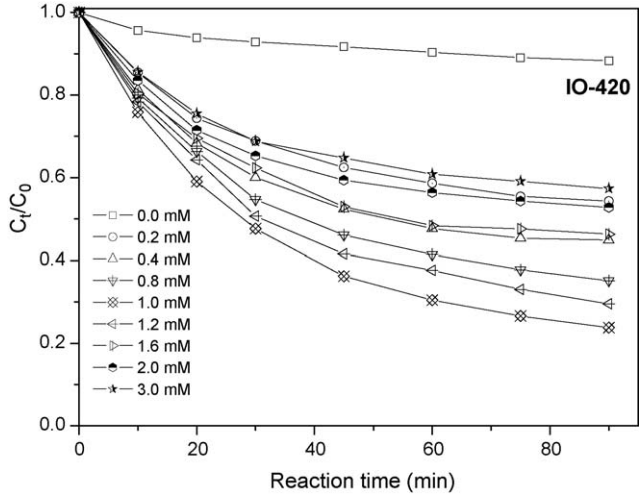

Fig. 5. The effect of initial concentration of oxalic acid on the photodegradation of 10 mg/L MBT under UV irradiation by using 0.4 g/L IO-420.

($R = 0.9707$) min^{-1} when the initial concentration of oxalic acid was 0, 0.2, 0.4, 0.8, 1.0, 1.2, 1.6, 2.0 and 3.0 mM, respectively. The results indicated that oxalate should significantly enhance MBT degradation and there was an optimal C^0_{ox} at 1.0 mM level for MBT degradation. When C^0_{ox} was less than the optimal one, MBT degradation would be promoted with the increase of C^0_{ox}, while MBT degradation would be limited with the increase of C^0_{ox} when C^0_{ox} was more than the optimal one. The similar results could also be obtained by using other iron oxides. Fig. 6 showed the dependence of the first-order kinetic constants k values for MBT photodegradation on C^0_{ox} by using γ-FeOOH, IO-250, IO-320, IO-420 and IO-520 with the dosage of 0.4 g/L. It is very interesting that the optimal initial concentrations of oxalic acid should be 1.0 mmol/L for all the five iron oxides and the k values were 0.75×10^{-2}, 2.01×10^{-2}, 2.74×10^{-2}, 1.84×10^{-2} and 1.50×10^{-2} min^{-1} in the presence of the optimal C^0_{ox} for γ-FeOOH, IO-250, IO-320, IO-420 and IO-520, respectively.

The above experimental results confirmed that the presence of iron oxides and oxalate in cooperation can greatly accelerate MBT degradation. While the first-order kinetic constant (k) was increased 12.5 times from 6.0×10^{-4} min^{-1} in the absence of oxalate to 7.5×10^{-3} min^{-1} in the presence of oxalate for γ-FeOOH, 28.7 times from 7.0×10^{-4} to 2.01×10^{-2} min^{-1} for IO-250, 34.3 times from 8.0×10^{-4} to 2.74×10^{-2} min^{-1} for IO-320, 16.7 times from 1.1×10^{-3} to 1.84×10^{-2} min^{-1} for IO-420 and 13.6 times from 1.1×10^{-3} to 1.5×10^{-2} min^{-1} for IO-520 with the optimal oxalate dosage. These results are very useful information to better understand the effect of oxalate on MBT degradation in such an iron oxide–oxalate complex system.

On the surface of iron oxides, oxalic acid is first adsorbed by iron oxide particles to form iron oxide–oxalate complexes of $[\equiv Fe^{III}(C_2O_4)_n]^{3-2n}$ as described by Eq. (1). $[\equiv Fe^{III}(C_2O_4)_n]^{3-2n}$ can be excited to form $[\equiv Fe^{II}(C_2O_4)_{(n-1)}]^{4-2n}$ and oxalate radical $(C_2O_4)^{\bullet -}$ as indicated by Eq. (2). In the solution, $[Fe^{III}(C_2O_4)_n]^{3-2n}$ could be also excited to form $[Fe^{II}(C_2O_4)_{(n-1)}]^{4-2n}$ and oxalate radical $(C_2O_4)^{\bullet -}$ as described by Eq. (3). The oxalate radical can be transferred into carbon-centered radical $(CO_2)^{\bullet -}$ as described by Eq. (4); and the excited electron is transferred from carbon-centered radical into adsorbed oxygen forming superoxide ion ($O_2^{\bullet -}$), as described by Eq. (5). Fe^{3+} reacts with $O_2^{\bullet -}$ to form O_2 and Fe^{2+} as described by Eq. (6) and Fe^{2+} reacts with $O_2^{\bullet -}$ to form H_2O_2 in acidic solution and Fe^{3+} as described by Eq. (7). To be important, Fe^{2+} is re-oxidized to Fe^{3+} in the presence of O_2. Fe^{2+} reacts with H_2O_2 to form hydroxyl radical ($^{\bullet}OH$) and Fe^{3+} as described by Eq. (8). Balmer and Sulzberger [30] reported Fe^{3+} mainly presented as $Fe(C_2O_4)_2^-$ and $Fe(C_2O_4)_3^{3-}$ in the Fe^{3+}-oxalate system when the concentration of oxalate was more than 0.18 mM. $Fe(C_2O_4)_2^-$ and $Fe(C_2O_4)_3^{3-}$ are much more efficiently photolyzed than other Fe^{3+} species. This was the reason why MBT photodegradation was enhanced greatly in the presence of oxalate. However, excessive oxalate would occupy the adsorbed sites on the surface of iron oxide and react competitively for hydroxyl radical. The adsorption of MBT on the surface was also hindered and only a part of hydroxyl radical would be utilized by MBT. On the other hand, a higher concentration of oxalate would lead to lower pH at the beginning which was not favorable to photo-Fenton system [47]. Thirdly, excessive oxalate would lead to the formation of a large amount of Fe^{3+}, which would inhibit the formation of H_2O_2, as described in Eq. (7). Therefore, excessive oxalate led to the inhibition of MBT degradation in the system. The reason for the difference of photochemical activity of the five kinds of iron oxides will be discussed behind.

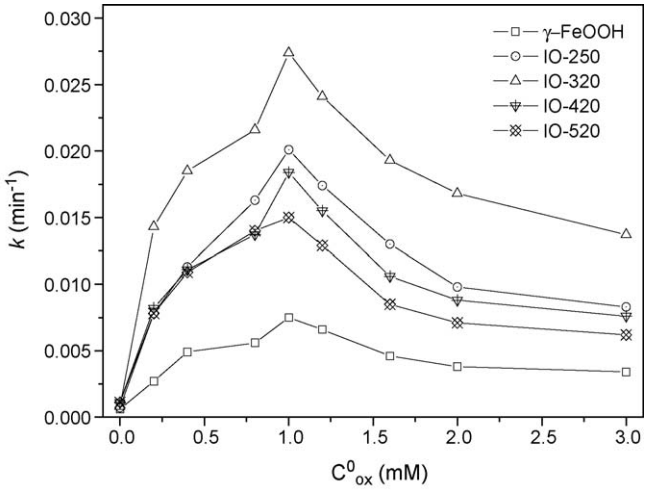

Fig. 6. The first-order reaction kinetic constants (k) vs. the initial concentration of oxalic acid (C^0_{ox}) in different iron oxides suspension with the dosage of 0.4 g/L under UV light irradiation.

$$\text{Iron oxide} + nH_2C_2O_4 \leftrightarrow [\equiv Fe(C_2O_4)_n]^{(2n-3)-} \quad (1)$$

$$[\equiv Fe(C_2O_4)_n]^{(2n-3)-} + h\nu \rightarrow Fe(C_2O_4)_2{}^{2-} \text{ (or } \equiv Fe(C_2O_4)_2{}^{2-}) + (C_2O_4)^{\bullet -} \quad (2)$$

$$Fe^{III}(C_2O_4)_n{}^{3-2n} + h\nu \rightarrow [Fe^{II}(C_2O_4)_{(n-1)}]^{4-2n} + (C_2O_4)^{\bullet -} \quad (3)$$

$$(C_2O_4)^{\bullet -} \rightarrow CO_2 + CO_2{}^{\bullet -} \quad (4)$$

$$CO_2{}^{\bullet -} + O_2 \rightarrow CO_2 + O_2{}^{\bullet -} \quad (5)$$

$$O_2{}^{\bullet -} + Fe^{3+} \rightarrow Fe^{2+} + O_2 \quad (6)$$

$$O_2{}^{\bullet -} + nH^+ + Fe^{2+} \rightarrow Fe^{3+} + H_2O_2 \quad (7)$$

$$Fe^{2+} + H_2O_2 \rightarrow Fe^{3+} + OH^- + {}^{\bullet}OH \quad (8)$$

3.5. The photodegradation of oxalate

Oxalic acid was the important factor affecting the photodegradation of MBT. The concentration of oxalate versus reaction time was shown in Fig. 7 in the presence of iron oxides with the dosages of 0.4 g/L when the initial concentration of oxalate was 1.0 mM. After 90 min reaction, the concentration of oxalate decreased to about 0.2–0.3 mM in all the five iron oxide–oxalate systems, and the first-order kinetic constants (k) for oxalate

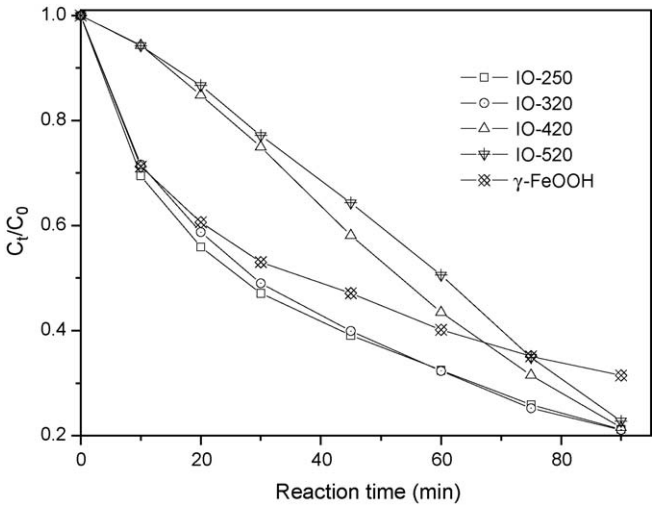

Fig. 7. The photodegradation of oxalic acid with the initial concentration of 1.0 mM in the presence of iron oxides with the dosage of 0.4 g/L under UV light irradiation.

degradation were 1.46×10^{-2} ($R = 0.9829$), 1.87×10^{-2} ($R = 0.9905$), 1.87×10^{-2} ($R = 0.9937$), 1.50×10^{-2} ($R = 0.9884$) and 1.37×10^{-2} ($R = 0.9802$) min^{-1} by using γ-FeOOH, IO-250, IO-320, IO-420 and IO-520, respectively. Oxalic acid should be removed in two ways. Firstly, oxalate was strongly adsorbed and complexed with the iron oxide as Eq. (1) [48,49]. Secondly, oxalate could be photodegraded by the $^{\bullet}OH$ generated as Eq. (9) [48]. Due to the high specific surface area and the less stable thermodynamically, γ-FeOOH, IO-250 and IO-320 can complex more easily with oxalic acid than IO-420 and IO-520. Therefore, the concentration of oxalic acid by using γ-FeOOH, IO-250 and IO-320 decreased quickly at first owing to adsorption on the surface and then became slowly while that decreased gradually during thorough the photochemical process by using IO-420 or IO-520.

$$^{\bullet}OH + HC_2O_4^- \rightarrow CO_2 + CO_2^{\bullet -} + H_2O \quad (9)$$

3.6. The variation of pH value

The dependence of the variation of pH versus reaction time on different initial concentration of oxalic acid by using IO-320 (0.4 g/L) was showed in Fig. 8A. Obviously, pH value increased along with the reaction time. At the beginning, a higher initial concentration of oxalic acid led to a lower initial pH value. However, the pH value in the solution increased much more slowly in the presence of a lower C_{ox}^0 than that of a higher one. A higher C_{ox}^0 also caused a greater increase of pH value in the solution with the reaction undergoing along. After 30 min reaction, the sequence of pH values from low to high turned reverse. A higher concentration of oxalic acid lead to more $[\equiv Fe(C_2O_4)_n]^{(2n-3)-}$ to be formed. But during the photochemical process, OH^- would be generated in accompany with the generation of $^{\bullet}OH$ as Eq. (10) [50,51]. More $[\equiv Fe(C_2O_4)_n]^{(2n-3)-}$ in the system can generate more OH^- so as to increase the pH value more in the solution in the later stage during the photochemical process.

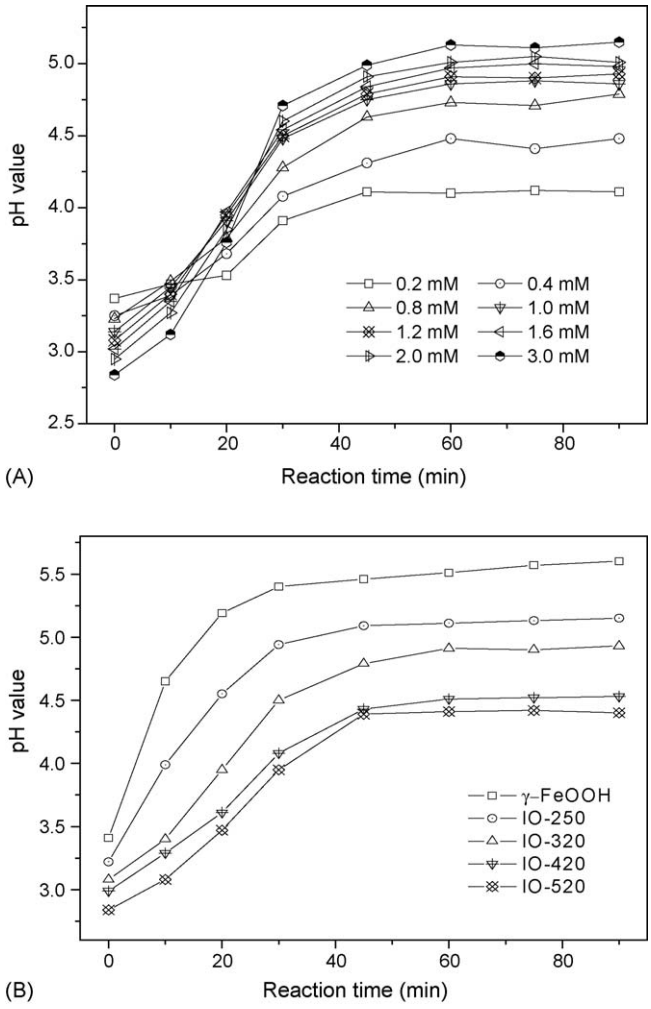

Fig. 8. The change of pH value during 10 mg/L MBT degradation process, with different C_{ox}^0 by using 0.4 g/L IO-320 (A) and with different iron oxides with the dosage of 0.4 g/L in the presence of 1.2 mM oxalic acid (B), under UV light irradiation.

$$Fe^{2+} + \equiv Fe(C_2O_4) + H_2O_2 \rightarrow Fe^{3+} + \equiv FeC_2O_4^+ + OH^- + {}^{\bullet}OH \quad (10)$$

The variation of pH also depended strongly on iron oxides as shown in Fig. 8B. The dosage of iron oxides was 0.4 g/L and the initial concentration of oxalic acid was 1.2 mM. The initial pH values were recorded after 30 min adsorption in dark, and were 3.41, 3.22, 3.08, 2.99 and 2.84 before UV light irradiation, and then increased to 5.60, 5.15, 4.93, 4.53 and 4.40 after 90 min reaction, by using γ-FeOOH, IO-250, IO-320, IO-420 or IO-520, respectively. When pH value of the reaction suspension was about 3, the photo-Fenton reaction was more active [52]. The higher initial pH value should be attributable to the stronger adsorption of oxalate on the surface of iron oxides. Obviously, the initial pH value in the solution was ranked the order as γ-FeOOH > IO-250 > IO-320 > IO-420 > IO-520. As above mentioned, the iron oxide that had a higher specific surface area and a lower stable thermodynamics can more easily complex

with oxalic acid and then more oxalic acid can be adsorbed which leading to a higher initial pH value in the solution. The increase of pH value was also resulted from the oxalate degradation. Fig. 8B showed that pH value increased quickly in the first 45 min reaction, and almost remained constant during 45–90 min reaction. And the increased amount of pH value also was ranked the order as γ-FeOOH > IO-250 > IO-320 > IO-420 > IO-520.

3.7. The formation of Fe^{2+} and Fe^{3+}

Fig. 9 showed the change of the concentration of Fe^{2+} (A) and Fe^{3+} (B) in the presence of different initial concentration of oxalic acid by using IO-320 with the dosage of 0.4 g/L under UV light irradiation. Obviously, the concentration of Fe^{2+} and Fe^{3+} depended strongly on the C^0_{ox}. A higher C^0_{ox} led to a higher concentration of Fe^{2+} and Fe^{3+}. As before mentioned, the excessive concentration of Fe^{3+} was also harmful to MBT photodegradation. Fig. 9 also showed that the concentration of Fe^{3+} dramatically increased and reached the peak while the concentration of Fe^{2+} were negligible after 30 min dark adsorption in the solution. The results showed that iron oxides can quickly be dissolved in oxalic acid solution and the reduction process of Fe^{3+} hardly happened in the dark. In the first 20 min during the photochemical process, the concentration of Fe^{2+} increased quickly and reached the peak because ≡Fe(III)-oxalate can be easily photo dissolved and reduced under UV light irradiation [17] and Fe^{2+} could be produced during this period as described by Eqs. (3) and (6). The formation of Fe^{2+} became slower with the decrease of the concentration of oxalic acid. At the same time, the pH value gradually increased due to the degradation of oxalic acid, and Fe^{3+} precipitated as $Fe(OH)_3$ with the increase of pH value, and then the concentration of Fe^{3+} decreased. At the meantime, Fe^{2+} would be consumed and Fe^{3+} formed in order to compensate Fe^{3+} because of the precipitation of Fe^{3+}, based on the Fenton-like reaction (Eqs. (7) and (8)). So, the concentration of Fe^{2+} decreased gradually in the later stage of the photochemical process.

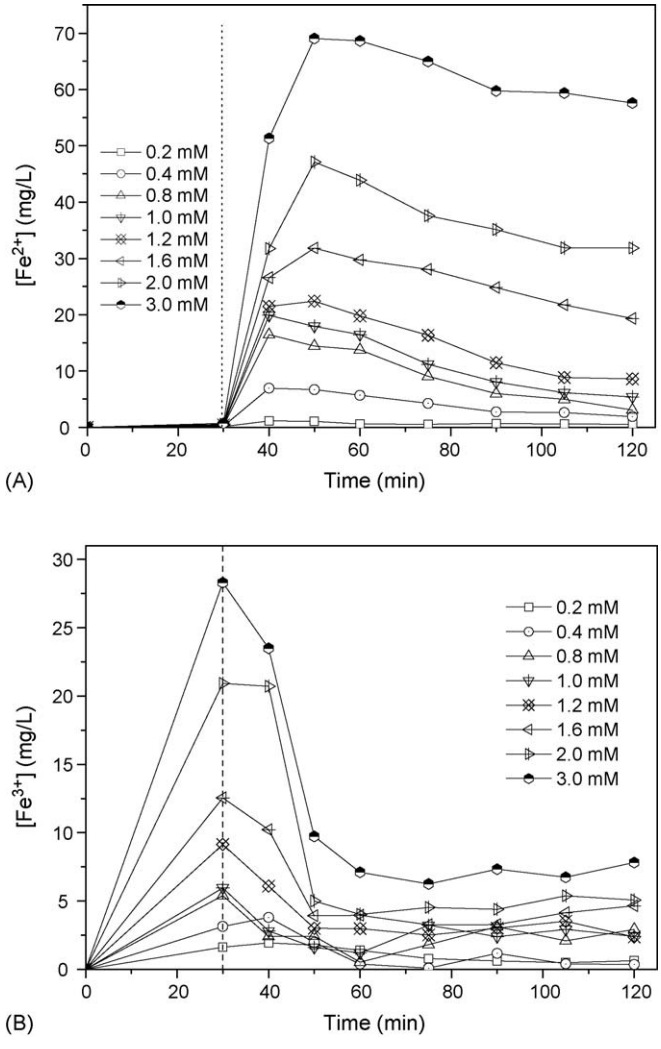

Fig. 9. The dependence of the change of concentration of Fe^{2+} (A) and Fe^{3+} (B) on different C^0_{ox} by using 0.4 g/L IO-320 under UV light irradiation.

Furthermore, the concentration of Fe^{2+} and Fe^{3+} in the iron oxide–oxalate system also depended on the iron oxides. As shown in Fig. 10, the concentration of Fe^{2+} (A) increased dramatically at the first 20 min for γ-FeOOH, IO-250 and IO-320 during the photochemical process and reached the peak value of 33.4, 25.5 and 22.4 mg/L, respectively, and then, decreased gradually on prolonging the reaction time. And the concentration of Fe^{3+} (B) increased to the peak value of 15.7, 11.3 and 9.1 mg/L, respectively, after 30 min dark adsorption and then decreased greatly and quickly, and remained constant after 30 min reaction. For IO-420 and IO-520, the concentration of Fe^{2+} increased gradually and was always below 2.5 mg/L during the whole photochemical process and the concentration of Fe^{3+} remained at about 1.0 mg/L level.

As above mentioned, IO-420 and IO-520 with pure α-Fe_2O_3 phase had the more stable thermodynamics and lower specific surface area than IO-250 and IO-320 which had the mixed phase of γ-Fe_2O_3 and α-Fe_2O_3, and than γ-FeOOH [17]. It is difficult to form ≡Fe(III)-oxalate complexes on the surface of IO-420 and IO-520, and then the concentration of dissolved iron in the solution was at low level. A lower concentration of ≡Fe(III)-oxalate complexes on the surface of iron oxides and Fe(III)-oxalate in the solution for IO-420 and IO-520 obviously led to a lower photochemical activity, while the excessive concentration of Fe^{3+} for γ-FeOOH and IO-250 also led to a lower photochemical activity for MBT degradation because the excessive amount of Fe^{3+} would inhibit the formation of H_2O_2, as described in Eq. (7). Many researchers had studied the effect of concentration of Fe^{2+} and Fe^{3+} on the degradation of organic pollutants in the photo-Fenton systems, and it was reported that both excess and lack of Fe^{2+} and Fe^{3+} would hinder the degradation of organic pollutants [53]. In the photo-Fenton reaction of this investigation, the concentration of Fe^{2+} and Fe^{3+} for IO-320 were more favorable to the reaction (7) and (8) than for γ-FeOOH and IO-250, and this led to a higher activity for IO-320 than for γ-FeOOH and IO-250.

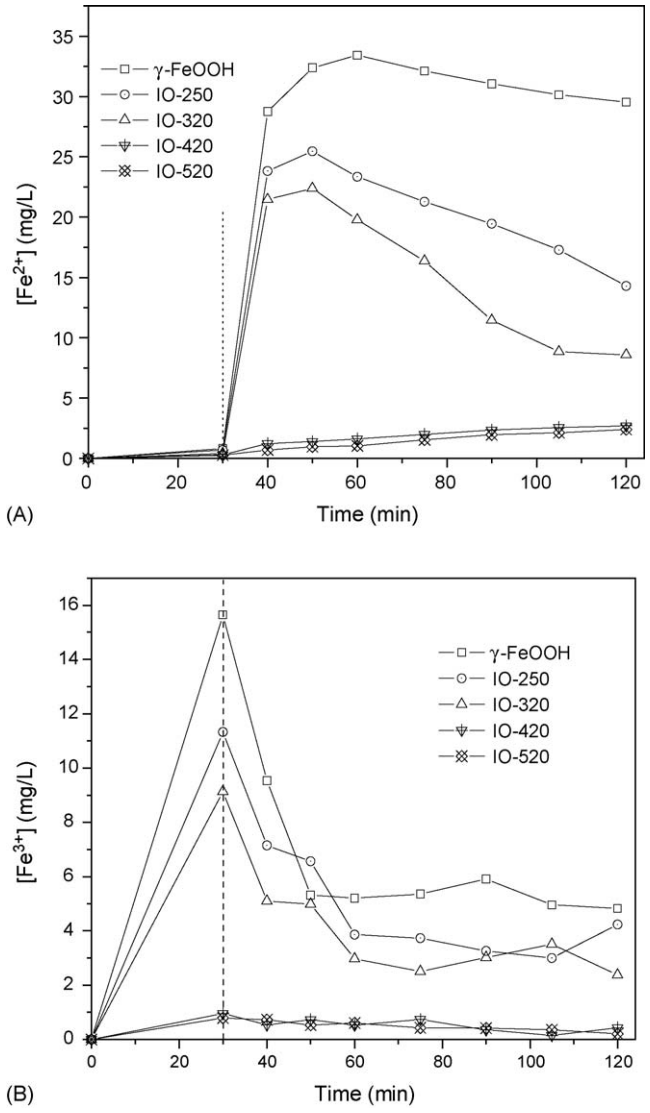

Fig. 10. The dependence of the change of concentration of Fe^{2+} (A) and Fe^{3+} (B) on different iron oxides with the dosage of 0.4 g/L in the presence of 1.2 mM oxalic acid under UV light irradiation.

4. Conclusions

The photodegradation of MBT depended strongly on the crystal structure, the dosages of iron oxides and the initial concentration of oxalate (C_{ox}^0). The optimal dosages for γ-FeOOH, IO-250, IO-320, IO-420 and IO-520 were 0.40, 0.35, 0.30, 0.25 and 0.25 g/L, respectively. And the optimal initial concentration of oxalic acid for all the five iron oxides was 1.0 mmol/L. IO-320 had the highest photochemical activity. The MBT photodegradation in the presence of optimal C_{ox}^0 was ranked the order as IO-320 > IO-250 > IO-420 > IO-520 > γ-FeOOH. The concentration of dissolved Fe^{2+} and Fe^{3+} depended strongly on the initial concentration of oxalic acid and iron oxides, and a higher C_{ox}^0 led to a higher concentration of Fe^{2+} and Fe^{3+}.

Acknowledgments

The authors wish to thank the China National Natural Science Foundation Project No. 20377011 and Guangdong Natural Science Foundation Key Project No. 036533.

References

[1] W.G. Barb, J.H. Baxendale, P. George, K.R. Hargrave, Trans. Faraday Soc. 47 (1951) 462.
[2] D.F. Bishop, G. Stern, M. Fleischmann, L.S. Marshall, Ind. Eng. Chem. Process Des. Dev. 7 (1968) 110.
[3] C. Walling, Acc. Chem. Res. 8 (1975) 121.
[4] C. Walling, K. Amaranth, J. Am. Chem. Soc. 104 (1982) 1185.
[5] M.C. Lu, J.N. Chen, C.P. Chang, J. Hazard. Mater. 65 (1999) 277.
[6] G.V. Buxton, C.L. Greenstock, W.P. Helman, A.B. Ross, J. Phys. Chem. Ref. Data 17 (1988) 513.
[7] J.E.F. Moraes, F.H. Quina, C.A.O. Nascimento, D.N. Silva, O. Chiavone-Filho, Environ. Sci. Technol. 38 (2004) 1183.
[8] R. Sauleda, E. Brillas, Appl. Catal. B 29 (2001) 135.
[9] J. Beltran-Heredia, J. Torregrosa, J.R. Dominguez, J.A. Peres, Chemosphere 42 (2001) 351.
[10] B. Gozmen, M.A. Oturan, N. Oturan, O. Erbatur, Environ. Sci. Technol. 37 (2003) 3716.
[11] J. Casado, J. Fornaguera, M.I. Galan, Environ. Sci. Technol. 39 (2005) 1843.
[12] J. Park, S. Kim, Y. Lee, K. Baek, J. Yang, Eng. Geol. 77 (2005) 217.
[13] H. Fallmann, T. Krutzler, R. Bauer, S. Malato, J. Blanco, Catal. Today 54 (1999) 309.
[14] K. Wu, Y. Xie, J. Zhao, H. Hidaka, J. Mol. Catal. A 144 (1999) 77.
[15] M. Pera-Titus, V. Garcia-Molina, M.A. Baños, J. Giménez, S. Esplugas, Appl. Catal. B 47 (2004) 219.
[16] E. Chamarro, A. Marco, S. Esplugas, Water Res. 35 (4) (2001) 1047.
[17] C. Siffert, B. Sulzberger, Langmuir 7 (1991) 1627.
[18] B.C. Faust, J. Allen, Environ. Sci. Technol. 27 (1993) 2517.
[19] Y.G. Zuo, Y.W. Deng, Chemosphere 35 (1997) 2051.
[20] U. Schwertmann, R.M. Cornell, Iron Oxides in the Laboratory: Preparation and Characterization, VCH, New York, 1991, pp. 14–18.
[21] T. Kayashima, T. Katayama, BBA-Gen. Subjects 1573 (2002) 1.
[22] R.V. Shende, V. Mahajani, Ind. Eng. Chem. Res. 33 (1994) 3125.
[23] A. Fortuny, C. Ferrer, C. Bengoa, J. Font, A. Fabregat, Catal. Today 24 (1995) 79.
[24] D. Duprez, F. Delanoe, J. Barbier Jr., P. Isnard, G. Blanchard, Catal. Today 29 (1996) 317.
[25] J.A. Zazo, J.A. Casas, A.F. Mohedano, M.A. Gilarranz, J.J. Rodriguez, Environ. Sci. Technol. 39 (2005) 9295.
[26] D. Mantzavinos, R. Hellenbrand, A.G. Livingston, I.S. Metcalfe, Appl. Catal. B 7 (1996) 379.
[27] Y.G. Zuo, J. Holgné, Environ. Sci. Technol. 26 (1992) 1014.
[28] R.G. Zepp, B.C. Faust, Environ. Sci. Technol. 26 (1992) 313.
[29] V. Nadtochenko, J. Kiwi, J. Chem. Soc. Faraday Trans. 93 (1997) 2373.
[30] M.E. Balmer, B. Sulzberger, Environ. Sci. Technol. 33 (1999) 2418.
[31] P. Mazellier, B. Sulzberger, Environ. Sci. Technol. 35 (2001) 3314.
[32] A. Bozzi, T. Yuranova, J. Mielczarski, A. Lopez, J. Kiwi, Chem. Commun. 19 (2002) 2202.
[33] H.W. Engels, H.J. Weidenhaupt, M. Abele, M. Pieroth, W. Hofmann, Ullmann's Encyclopedia of Industrial Chemistry, vol. 112, fifth ed., Wiley–VCH, Wenheim, p. 329.
[34] C.C. Chen, C.E. Lin, Anal. Chim. Acta 321 (1996) 215.
[35] Anon., 2-Mercaptobenzothiazole; proposed test rule, Federal Register 50 (1985) 46121.
[36] O. Fiehn, G. Wegener, J. Jochimshn, M. Jekel, Water Res. 32 (1998) 1075.

[37] M.A. Gaja, J.S. Knapp, Water Res. 32 (1998) 3786.
[38] M.H. Habibi, S. Tangestaninejad, B. Yadollahi, Appl. Catal. B 33 (2001) 57.
[39] M.A. Malouki, C. Richard, A. Zertal, J. Photochem. Photobiol. A 167 (2004) 121.
[40] F.B. Li, X.Z. Li, M.F. Hou, K.W. Cheah, W.C.H. Choy, Appl. Catal. A 285 (2005) 181.
[41] F.S. Yen, W.Ch. Chen, J.M. Yang, Ch.T. Hong, Nano Lett. 2 (2002) 245.
[42] Joint Committee for Powder Diffraction Standards, "JCPDS" International Center for Diffraction Data, 1979.
[43] J.G. Yu, J.C. Yu, M.K.-P. Leung, W.K. Ho, B. Cheng, X.J. Zhao, J.C. Zhao, J. Catal. 217 (2003) 69.
[44] C. Paipa, M. Mateo, I. Godoy, E. Poblete, M.I. Toral, T. Vargas, Miner. Eng. 18 (2005) 1116.
[45] R.M. Cornell, U. Schwertmann, The Iron Oxides: Structure, Properties, Reaction, Occurrences and Uses, second ed., Wiley–VCH, Weinheim, 2003, pp. 29–31.
[46] J.K. Leland, A.J. Bard, J. Phys. Chem. 91 (1987) 5076.
[47] L. Lunar, D. Sicilia, S. Rbio, D. Perez-Bendito, U. Nickel, Water Res. 34 (2000) 1791.
[48] B. Sulzberger, H. Laubscher, Mar. Chem. 50 (1995) 103.
[49] R.M. Smith, A.E. Martell, Critical Stability Constants: Inorganic Complexes/Other Organic Ligands, vol. 4, Plenum Press, New York, 1976.
[50] K.A. Hislop, J.R. Bolton, Environ. Sci. Technol. 33 (1999) 3119.
[51] J.D. Rush, B.H.J. Bielski, J. Phys. Chem. 89 (1985) 5062.
[52] F.J. Rivas, V. Navarrete, F.J. Beltran, J.F. Garcia-Araya, Appl. Catal. B 48 (2004) 249.
[53] M. Pera-Titus, V. Garcia-Molina, M.A. Banos, J. Gimenez, S. Esplugas, Appl. Catal. B 47 (2004) 219.